SLEEPJ, 2019, 1–15

doi: 10.1093/sleep/zsy201
Advance Access Publication Date: 27 October 2018
Original Article

ORIGINAL ARTICLE

Sleep disruption elevates oxidative stress in parvalbumin-positive cells of the rat cerebral cortex

John H. Harkness[1,*], Priyanka N. Bushana[2], Ryan P. Todd[1], William C. Clegern[2], Barbara A. Sorg[1] and Jonathan P. Wisor[2]

[1]Department of Integrative Physiology and Neuroscience, Translational Addiction Research Center, Washington State University, Vancouver, WA and [2]Department of Biomedical Sciences, Elson S. Floyd College of Medicine, Spokane, WA

*Corresponding author. Jonathan Wisor, Department of Biomedical Sciences, Elson S. Floyd College of Medicine, Washington State University, Spokane, 412 E Spokane Falls Blvd, Spokane, WA 99202. Email: j_wisor@wsu.edu.

Abstract

We used a novel automated sleep disruption (SD) apparatus to determine the impact of SD on sleep and molecular markers of oxidative stress in parvalbumin (PV) neurons in the rat prefrontal cortex (PFC). Rats were subjected to two 6 hr SD sessions from zeitgeber time (ZT) 0 to ZT6, one by the gentle handling method and the other by an automated agitator running the length of the rat's home cage floor (a novel SD method). The same rats were later subjected to a 12 hr SD session from ZT0 to ZT12. Sleep was disrupted with both methods, although rats slept less during gentle handling than during the automated condition. Immediately after both SD sessions, rats displayed compensatory sleep characterized by elevated slow-wave activity. We measured in the prelimbic prefrontal cortex (prelimbic PFC; 6 and 12 hr SD) and orbital frontal cortex (12 hr SD) the intensity of the oxidative stress marker, 8-oxo-2′-deoxyguanosine (8-oxo-dG) as well as the staining intensity of PV and the PV cell-associated perineuronal net marker, *Wisteria floribunda* agglutinin (WFA). In the prelimbic PFC, 6 hr SD increased the intensity of 8-oxo-dG, PV, and WFA. After 12 hr SD, the intensity of 8-oxo-dG was elevated in all neurons. PV intensity was elevated only in neurons colabeled with 8-oxo-dG or WFA, and no changes were found in WFA intensity. We conclude that in association with SD-induced sleep drive, PV neurons in the prelimbic PFC exhibit oxidative stress.

Statement of Significance

Sleep deprivation has been associated with significant health consequences and disruption to the normal function of the brain in humans and animals. Here, using a novel sleep disruption method, we found that sleep disruption led to increased oxidative stress and parvalbumin content in neurons. In some cases, sleep disruption also led to increased perineuronal nets around these neurons. These data are the first to show a relationship between sleep disruption and neurochemical changes specific to parvalbumin neurons.

Key words: sleep deprivation; EEG spectral analysis; biological rhythms; cellular and molecular biology; neuroanatomy; animal models

Submitted: 26 April, 2018; **Revised:** 6 August, 2018

Introduction

Despite such clear counter indications, sleep disruption is an increasingly common concern. A report commissioned by the Centers for Disease Control and Prevention tracked changes in sleep habits in the American public from 1985 to 2011. Over this time, the percentage of adults reported to sleep less than 6 hr per night nearly doubled from 38 million to 70 million [1]. Sleep deprivation compromises prefrontal cortex (PFC)-dependent reward-related behavior and its cellular-level correlate: long-term potentiation of PFC circuits [2, 3] in rodent models. Additional work is needed to understand the pathophysiology underlying this effect of sleep deprivation.

Protracted wake is associated with signs of increased oxidative stress, both in the blood plasma of human subjects [4] and the brain tissue of animals post mortem [5–7]. Oxidative stress occurs in neurons as a product of metabolic activation secondary to excitation [8, 9]. Whether specific populations of wake-activated neurons within the cerebral cortex are especially vulnerable to oxidative stress during sustained wake is uncertain. One population of interest in this context is parvalbumin (PV) containing fast-spiking GABAergic interneurons, which express Fos—a marker for neuronal activation, in the medial prefrontal cortex [10] and sensory cortex [11] of animals that have engaged in exploratory behaviors. The functioning of PV cells may be particularly vulnerable to oxidative stress during sleep deprivation, given the high rate of firing that these cells must undergo to produce gamma activity, a prominent feature of the waking brain [12]. In fact, the observed decline in gamma activity in local field potentials of the rodent cerebral cortex across sustained wake [13] may be a readout of oxidative stress in PV cells: increasing oxidative stress suppresses gamma activity in neural cultures containing PV cells [14, 15].

Many PV cell bodies and proximal dendrites are encased by unique aggregations of extracellular matrix (ECM), called perineuronal nets (PNNs). The role of PNNs in normal brain function has gained attention because of their reported importance in brain plasticity, as occurs during critical periods of development and in the formation of memories [16, 17]. Perineuronal nets have also been implicated in disorders and pathologies, such as recovery from nerve damage, schizophrenia, Alzheimer's disease, stroke, epilepsy, fear memory, and drug addiction [18–23]. PNNs protect neurons from oxidative stress [15, 24] perhaps by limiting GABAergic interneuron excitability. Chondroitin sulfates, which make up the bulk of material in PNNs, are substrates for oxidation/reduction reactions that act as a source of protection against oxidative stress [25, 26]. This protection has implications for how sleep deprivation may alter cognitive function because PV cells drive gamma oscillations that promote cognitive processing [27, 28]. Importantly, PNNs themselves are also susceptible to the effects of excessive oxidative stress [15].

Here we tested the hypotheses that oxidative stress precipitated by sustained wake would (1) elevate the oxidative stress marker 8-oxo-2′-deoxyguanosine (8-oxo-dG) in PV cells and (2) modify the intensity of PNN staining in the PFC. We assessed the generalizability of this response across cell types and brain regions by measuring (8-oxo-dG) in both PFC and orbital frontal cortex (OFC), both within immunohistochemically identified PV cells and pan-cellularly. We measured the polysomnographic response and histological markers for oxidative stress, PV, and PNNs after 6 and 12 hr sleep disruption (SD) and spontaneous sleep (SS). We determined that, in the prelimbic PFC, 6 hr SD increased oxidative stress in PV cells and increased the staining intensity of PV and *Wisteria floribunda* agglutinin (WFA). Similarly, 12 hr SD increased 8-oxo-dG within all cells, including within a subset of cells containing PV in the prelimbic PFC, with far smaller changes occurring in the OFC. Furthermore, PV intensity in the prelimbic PFC increased after 12 hr SD. The staining intensity of PNNs (using WFA) was not different after 12 hr SD in either brain region. These findings are consistent with previous studies that demonstrate increases in oxidative stress in the brain but further identify a cortical cell population in the prelimbic PFC that is particularly sensitive to the oxidative stress-inducing effect of SD.

Methods

Automated sleep disruption apparatus

We designed a method for automated sleep disruption (ASD) using a novel Sleep Fragmentation Platform (Rewire Neuroscience, LLC; Portland, OR. Detailed description available at https://RewireNeuro.com). This sleep disruption system is designed to receive an unmodified rodent home cage onto the apparatus platform. The home cage is placed on top of the Sleep Fragmentation Platform (25.4 × 53.34 cm) allowing linear movement back and forth under the length of the home cage. A linearly cycling agitator is placed within the home cage, and functions to physically disturb the rodent, thus preventing sleep. Through magnetism, the platform pulls the agitator along the cage floor, causing the agitator's wheels to roll. The agitator moves in alternating directions in a linear path along the length of the rodent home cage. In the current experiments, speed was set at approximately 2.54 cm/s.

Shielded DC electronics on the platform communicate over an RJ45 "Ethernet-style" cable with a specially designed computer. By removing AC components from the Sleep Fragmentation Platform, we find fewer artifacts and less noise collected during EEG recording compared with other ASD methods available. Additionally, we have not found interference resulting from the use of magnets in our platform design. Linear bidirectional movement of the agitator was used during the 6 hr ASD experiments, and randomized movement of the agitator was used for the duration of the 12 hr ASD experiments. During randomized movement, the agitator randomly changes direction or stops (for no longer than 1 s), thus reducing the possibility that the rodent habituates to the sound or movement of the agitator. Once an unpredicted or "randomized" movement has occurred, the agitator completes one full lap of the chamber before randomized movement is again possible. Requiring an agitator travel fully between random events eliminates the potential for one end of the chamber to become an undisturbed zone.

Polysomnographic instrumentation, recording, and data analysis

All experiments were performed under an Institutional Animal Care and Use Committee-approved protocol and in accordance with the National Research Council guidelines and regulations controlling experiments in live animals [29]. Male Sprague-Dawley albino rats were purchased from Simonsen Laboratories

(Gilroy, CA) at 200 g. At all times, they were individually housed under 12:12 (L:D) hr conditions at a temperature of 22–24°C with unrestricted access to food and water. Rats were instrumented for polysomnographic measurement under isoflurane anesthesia (induction 5% and maintenance 1%–3% to maintain breathing at 0.5–1 Hz) using standard laboratory procedures [30, 31], as follows. The fur was shaved from the top of the skull. The shaved area extended laterally from ear to ear and anterior–posterior from the eyes to the posterior end of the skull. The exposed skin was cleansed with betadine followed by ethanol. A medial incision was made on the skin atop the skull, from between the eyes to the back of the skull. The bone surface was cleansed with hydrogen peroxide and sterile saline. Stereotaxic coordinates were established based on bregma and lambda. Holes were made with a high-speed dental drill with a 0.5 mm ball burr bit to establish each implantation site in the skull. Two frontal screws were placed 1.5 mm lateral to the midline and 1 mm anterior to bregma. The left frontal screw served as an internal ground. The two parietal screws were placed 1.5 mm lateral to the midline and approximately 2 mm anterior to lambda. Parietal electrode locations relative to skull landmarks were approximate to accommodate to the connector apparatus. A screw electrode located over the cerebellum served as a ground. EEG screws (0.8 mm in length, with 2 cm of uncoated 30-gauge tinned-copper bus wire presoldered to screw head) were screwed into the holes with a slotted hand screwdriver for approximately 4–5 revolutions to obtain the desired depth. Once EEG screws were positioned in the skull, they were bonded with dental acrylic cement (Lang Dental—Ortho-Jet cement), with the ends of the wires emanating from EEG leads exposed. A plastic six-pin plug interface (Plastics One; Roanoke, VA) was positioned above the dried cement mound. Wire ends were soldered to the contacts on the plastic connector. The wire leads and the base of the plastic connector were encased in cement. For neck electromyogram, wires were embedded bilaterally beneath the nuchal musculature. A double surgeon's knot of 5-0 nylon suture was placed around these wires just distal to where they exited the muscle. The skin that was retracted to access the skull and muscle tissue was closed with single-interrupted surgeon knots, using a reverse cutting P-3 needle and 5-0 nylon suture. Buprenorphine was administered as an analgesic (0.1 mg/kg, subcutaneous) and flunixin meglumine (0.1 mg/kg, subcutaneous) as an anti-inflammatory.

Experimental design

Two experiments were performed. In the first experiment, EEG recordings were taken throughout the duration of SD (6 hr) and for the immediate subsequent 6 hr. For this experiment, rats were subjected to both 6 hr ASD and 6 hr gentle-handling SD (GHSD) from ZT0 to ZT6 in a counterbalanced design, and EEG data were compared with their baseline values collected at the same time of day on the day prior to SD ($N = 8$). Subsequently, another baseline was collected, and all rats were either subjected to 12 hr ASD from ZT0 to ZT12 ($N = 4$) or allowed to sleep spontaneously ($N = 4$). During this 12 hr period, EEG recordings were collected. Rats were killed immediately after the 12 hr ASD to determine the intensity of 8-oxo-dG, PV, and PNN expression in both the prelimbic PFC and the OFC. In a second experiment, we determined whether a shorter SD period of 6 hr would preferentially produce oxidative stress in PV cells. For this experiment, rats were subjected to 6 hr ASD ($N = 4$) or allowed to sleep spontaneously ($N = 4$); no EEG recordings were taken. These rats were killed immediately after the 6 hr ASD from ZT0 to ZT6 to determine the intensity of 8-oxo-dG, PV, and PNN expression in the prelimbic PFC.

In the first experiment, before EEG recordings were collected, rats were subjected to overnight acclimation to the tethering and the recording environment in a 35.56 × 53.34 × 86.36 cm plastic home cage, identical to colony housing, except with an open lid for tethering and an agitator placed within the cage. EEG and EMG potentials were collected at 400 Hz beginning at light onset, after the overnight acclimation. Animals were undisturbed during a 24 hr baseline recording session, then subjected to the first of two SD sessions beginning at ZT0: by either the GHSD or ASD method. SD was followed by a 6 hr recovery session from ZT6 to ZT12, ending at dark onset, during which animals were allowed to sleep spontaneously. The second SD session was initiated 42 hr after the end of the first. This session counterbalanced the SD applied in the first session: rats were subjected to the opposite SD method from what they experienced in the first SD session. Again, this session was followed by a 6 hr recovery session ending at dark onset.

After rats had undergone 6 hr SD by both methods, they were subjected to the terminal SD experiment. This experiment was conducted 5 days after the most recent SD session for half of the subjects and 19 days after the most recent SD session for the other half of the subjects. Baseline polysomnographic data were collected first, and then throughout a final 12 hr session, from ZT0 to ZT12, half of the rats ($N = 4$) were subjected to 12 hr SD via the ASD method, beginning at light onset and immediately euthanized by a pentobarbital overdose (50 mg/kg under brief, <1 min, 5% isoflurane exposure) at the end of the SD session. The other half of the rats ($N = 4$) were allowed to sleep spontaneously (SS) for 12 hr from ZT0 to ZT12 before being euthanized by pentobarbital overdose (50 mg/kg under brief, <1 min, 5% isoflurane exposure).

In the second experiment, surgically naïve, noninstrumented rats were subjected to overnight acclimation to the agitator (placed within their home cage and unmoving) with a cage lid that contained food and water. Animals were undisturbed during a 24 hr habituation session and then subjected to 6 hr of ASD ($N = 4$) or SS ($N = 4$). Rats were immediately euthanized by isoflurane exposure and perfused at the end of the 6 hr session.

Data collection and processing

EEG and EMG potentials were collected at 400 Hz using the Pinnacle Technology rodent polysomnographic system (Lawrence, KS) as detailed elsewhere [32, 33]. Data were converted to European data format (edf) by Pinnacle Technology's Sirenia software. State classification was done with Neuroscore 3.0 software as detailed elsewhere [32–34]. The vigilance states of wakefulness, slow-wave sleep (SWS), and rapid eye movement sleep (REMS) were classified in 10 s epochs by an experienced scorer blinded to the experimental conditions. Waking state was further subclassified as either quiet wakefulness (QW; those epochs in which the root mean square of the EMG signal in the epoch was ≤33rd percentile of root mean square values across all wake epochs in the recording) or active wakefulness

(AW; those epochs in which the root mean square of the EMG signal in the epoch was ≥66th percentile of root mean square values across all wake epochs in the recording). All other epochs of wake (EMG root mean square > 33rd percentile and < 66th percentile) were classified as intermediate wakefulness (IW). EEG spectral data were processed with the MATLAB computing language. Data were high-pass filtered at 0.01 Hz and band-stop filtered at 60 Hz with the MATLAB filtfilt function. EEG data were subjected to discrete Fourier transform using the MATLAB FFT function [35]. Slow-wave activity (SWA) during SWS (EEG power in the 1–4 Hz range) was normalized to the average SWA value across all epochs of SWS in the baseline 24 hr recording immediately prior to the first SD session. For the purpose of calculating mean episode durations and the total number of episodes, an episode of any given state was initiated by at least three consecutive epochs of a given state and terminated by a single epoch of any other state. Instances where only one or two consecutive epochs of a state occurred were thus not included in tallying episode numbers or episode mean durations. Sleep state timing and EEG parameters were populated onto spreadsheets via a custom MATLAB algorithm created by the authors [13, 36, 37] and were then subjected to statistical analyses with Dell Statistica 13.2 (2016) and GraphPad Prism 7.

Immunohistochemistry

Upon reaching complete unresponsiveness from pentobarbital overdose, rats were perfused transcardially with 150 mL 1× PBS per rat at a rate of 300 mL/min. Perfusate was switched to 4% paraformaldehyde and perfused at the same rate for at least 250 mL/rat. Brains were removed, immersed in 20 mL 4% paraformaldehyde overnight, and then immersed in 20% sucrose in PBS solution and refrigerated. After 2 days in sucrose solution (when the brains sank), brains were flash-frozen with powdered dry ice and stored at –20°C until sectioned.

Coronal sections containing the prelimbic PFC or OFC (PFC; +4.0 through +3.6 from bregma) were collected on a freezing microtome at 40 µm for a 1:8 section series [35]. Triple-staining was performed by first washing a single series of free-floating sections three times for 5 min in PBS. Tissue was then quenched in 50% ethanol for 30 min. Sections were then washed in PBS three times for 5 min each, before being placed in a blocking solution containing 3% normal goat serum (Vector Laboratories) for 1 hr. Subsequently, tissue was coincubated with rabbit-anti-PV (1:1000; ThermoFisher Scientific) and mouse-anti-8-oxo-dG primary (1:350; EMD Millipore) antibodies, and 2% normal goat serum at 4°C overnight. Tissue was then rinsed in PBS three times for 10 min each and incubated for 2 hr in secondary antibody (goat antirabbit Alexa Fluor 405 for the PV antibody and goat antimouse Alexa Fluor 594 for the 8-oxo-dG antibody), and 2% normal goat serum. Again, tissue was washed in PBS three times for 10 min each and then incubated with the fluorescein-labeled PNN marker, WFA (1:500; Vector Laboratories) and 2% normal goat serum at 4°C overnight. After three 10 min washes in PBS, sections were transferred to mounting media and then mounted onto Superfrost Plus slides and allowed to dry overnight. After drying, ProLong Gold Antifade Mountant (ThermoFisher Scientific) was applied to the slides before coverslipping. Slides were stored flat and allowed to dry for 3 days before imaging.

Quantification of immunohistochemical images

Imaging was performed on a Leica SP8 laser scanning confocal microscope with an HCX PL apo CS, dry, 20× objective with 0.70 numerical aperture.Four hundred five, 488, and 594 nm lasers were used for excitation and were detected by three photomultiplier tubes in the 400–450, 460–510, and 590–640 nm ranges, respectively. Calibration of the laser intensity, gain, offset, and pinhole settings was determined within the OFC of a control animal, as this region most reliably expresses strong WFA staining. These settings were maintained for all images. Images were collected in z-stacks of 20 images each (step size 0.44 µm; containing the middle 8.45 µm of each 40 µm section), encompassing the prelimbic PFC and OFC.

All images (1.194 pixels/µm) were compiled into summed images using ImageJ macro plug-in Pipsqueak (https://labs.wsu.edu/sorg/research-resources/), scaled, and converted into 8-bit, grayscale, tiff files. Pipsqueak was run in "semi-automatic mode" to select ROIs to identify individual PV+ cells, PNNs, and 8-oxo-dG-labeled cells, which were then verified by a trained experimenter who was blinded to the experimental conditions. The plug-in compiles this analysis to identify single- [38], double-, and triple-labeled neurons (Harkness et al., unpublished data; https://ai.RewireNeuro.com). Control group mean cell intensities were used to calculate normalized intensities for each label, respectively. Distributions of normalized intensities were then compared between experimental groups, within stain type, using the two-sample Kolmogorov–Smirnov test to assess changes in the distribution of intensities between SD and control rats. To determine the number of cells expressing each combination of stains, the number of cells was averaged for each animal and the results were subjected to a two-way ANOVA (treatment x stain type). For all analyses, statistical significance was set at $p < 0.05$.

Results

Sleep loss and recovery: comparison of 6 hr GHSD and 6 hr ASD conditions

Under baseline conditions, animals spent 224 ± 48 min in SWS and 34 ± 18 min in REMS across the 6 hr interval beginning at lights-on (ZT0–ZT6). Experimental condition had significant main effects on time spent in SWS ($F_{2,14} = 54.8$, $p < 0.001$) and REMS ($F_{2,14} = 21.0$, $p < 0.001$; Table 1). Sleep loss during SD was a result of increased time spent in both intermediate wake ($F_{2,14} = 58.9$, $p < 0.001$) and active wake ($F_{2,14} = 14.4$, $p < 0.001$; Table 1). Time spent in quiet wake was not altered in either SD condition relative to baseline ($F_{2,14} = 1.5$, $p = 0.260$; Table 1). There was a significant condition × time interaction affecting SWS ($F_{10,70} = 3.5$, $p < 0.001$), but not REMS ($F_{10,70} = 1.5$, $p = 0.157$). SWS occurred with increasing frequency across time in SD (Figure 1A), to a greater extent in the ASD condition than in the GHSD condition. Consequently, the amount of SWS was significantly greater in ASD than GHSD during hours 2–6 of SD. Although condition × time interaction was not significant for REMS, REMS was detected in 2, 3, and 5 rats, respectively, in the final 3 hr of ASD (Figure 1B). REMS was not detected in any rats throughout the duration of the 6 hr GHSD session.

EEG spectral power was altered as a consequence of SD by either method (Figures 2 and 3). SWA occurring in epochs of

Table 1. Percentage of time spent in each sleep state during a 6 hr ASD session, a 6 hr GHSD session, and 6 hr of SS (ZT0–6)

State	ASD (% of total time)	GHSD (% of total time)	SS (% of total time)
SWS	27 ± 7*,**	3 ± 2*	62 ± 13
REMS	2 ± 2*	0 ± 0*	10 ± 5
Quiet Wake	23 ± 12	25 ± 8	15 ± 7
Intermediate Wake	28 ± 5**	37 ± 5*	7 ± 3
Active Wake	22 ± 8**	35 ± 10*	7 ± 3

*$p < 0.05$ difference between SD and SS, Fisher's LSD.
**$p < 0.05$ difference between ASD and GHSD, Fisher's LSD.

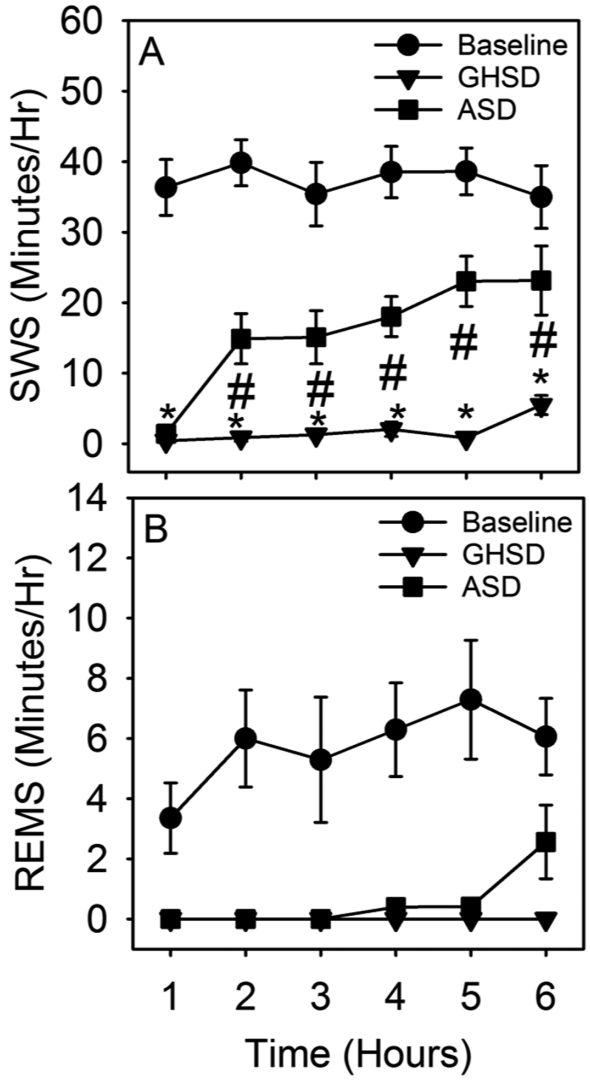

Figure 1. SWS and REMS recorded during 6 hr GHSD or ASD. (A) Time spent in SWS during the 6 hr SD session. #$p < 0.05$, Fisher's LSD, ASD vs. GHSD. *$p < 0.05$, Fisher's LSD, for both GHSD vs. baseline and ASD vs. baseline. (B) Time spent in REMS during the 6 hr SD session. Post hoc comparisons were not done on an hourly basis for REMS due to nonsignificant condition × time interaction.

quiet wake was elevated during the 6 hr ASD session, but not the GHSD session, relative to the analogous time of day in the baseline recording (main effect of condition $F_{2,14} = 6.0$, $p = 0.016$; Figure 2). SWA was significantly elevated in SWS in the hours subsequent to both GHSD (by 45 ± 8% in hour 1 post-SD) and ASD

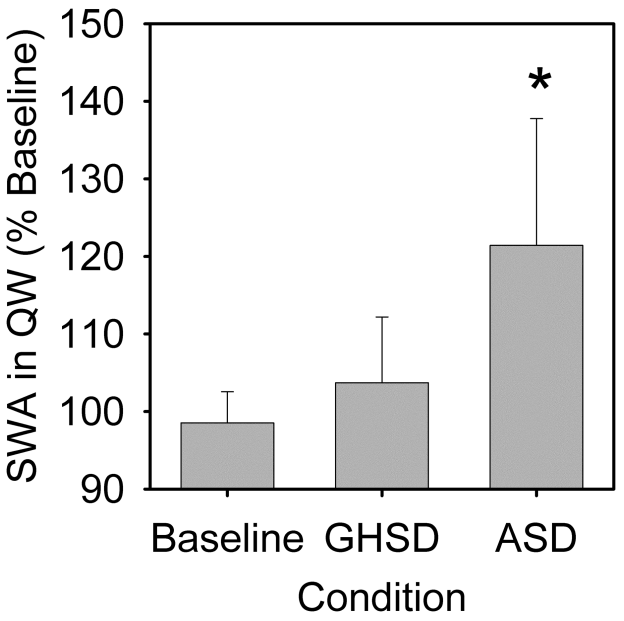

Figure 2. Slow-wave activity in the quiet waking EEG. Values are averages of all QW epochs detected in the entire 6 hr ASD interval, entire 6 hr GHSD interval, or the equivalent time of day on the baseline day and are reported as a percentage of the average SWA across all QW epochs in the entire baseline recording. *$p < 0.05$, Fisher's LSD, ASD vs. baseline.

(by 21 ± 16% in hour 1 post-SD) relative to the analogous time of day in the baseline recording (Figure 3B). There was additionally a condition × time interaction. Although SWA during SWS was elevated in both SD conditions relative to baseline throughout 6 hr of post-SD recording, it was elevated to a greater extent in GHSD than in ASD during hours 1–2 post-SD. After this time, SWA was elevated to the same extent in both GHSD and ASD relative to baseline.

In a separate group of animals, 6 hr ASD significantly increased the mean intensities of cells single-labeled for 8-oxo-dG in the prelimbic PFC compared with rats in the SS control condition (Figure 4A). The distributions of ($D = 0.2504$, $p < 0.0001$), PV ($D = 0.1897$, $p < 0.0001$), and WFA ($D = 0.1243$, $p < 0.0005$) -labeled populations were shifted to the right, indicating increased signal intensity, in 6 hr ASD-treated rats compared with SS (Figure 4B).

We also measured double-labeled cells for staining intensity. The intensity of 8-oxo-dG was elevated following 6 hr ASD treatment in PV cells ($D = 0.2864$, $p < 0.0001$) and in cells surrounded by WFA ($D = 0.2351$, $p < 0.0001$) (Figure 4, C and D). Here again, 6 hr ASD treatment resulted in rightward shifts of intensity of 8-oxo-dG in PV cells and in WFA-surrounded cells. ASD treatment also significantly increased the intensity of PV colocalized with 8-oxo-dG ($D = 0.2076$, $p < 0.0001$), or WFA ($D = 0.2585$, $p < 0.0001$) in the prelimbic PFC compared with SS control, and ASD shifted PV intensity distributions rightward. Both PV+ and PV– cells showed a 25%–26% increase of 8-oxo-dG after 6 hr SD, compared with controls. Additionally, 8-oxo-dG staining in PV+ cells was 27% higher than in PV– cells of 6 hr sleep-disrupted rats. WFA intensity was elevated around cells colocalized with 8-oxo-dG ($D = 0.1104$, $p < 0.05$) or PV ($D = 0.147$, $p < 0.05$) in the prelimbic PFC of ASD compared with SS control rats. WFA intensity distributions of ASD rats were shifted upward around 8-oxo-dG cells and rightward around PV cells.

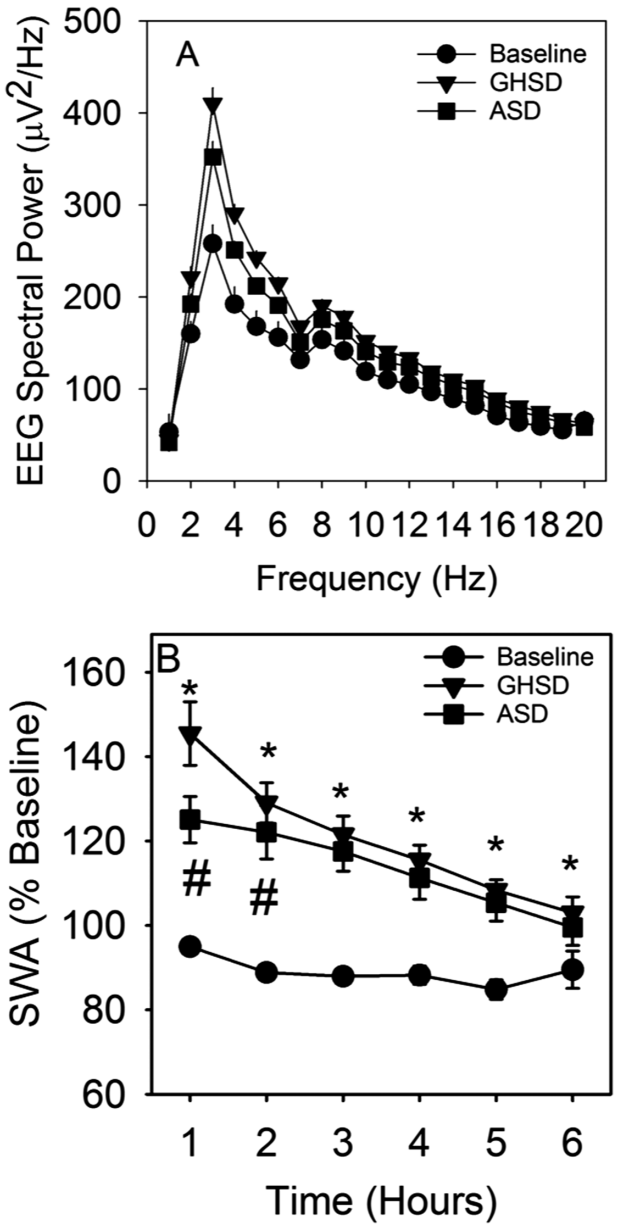

Figure 3. EEG spectral power in SWS subsequent to SD. (A) EEG power in 1 Hz bands, averaged across all SWS epochs in the 1 hr interval immediately after termination of ASD or GHSD and the equivalent time of day on the baseline day. (B) Slow-wave activity (1–4 Hz) in the SWS EEG in the 6 hr interval immediately after termination of ASD or GHSD and the equivalent time of day on the baseline day. Values in B are reported as a percentage of the average SWA from all SWS epochs in the entire baseline recording. #$p < 0.05$, Fisher's LSD, ASD vs. GHSD. *$p < 0.05$, Fisher's LSD, GHSD vs. baseline and ASD vs. baseline.

In triple-labeled cells of the prelimbic PFC, ASD increased the intensity of 8-oxo-dG and shifted it rightward in cells that were triple-labeled for 8-oxo-dG, PV, and WFA ($D = 0.2695$, $p < 0.0001$; Figure 4, E and F). Additionally, PV intensity colocalizing with 8-oxo-dG and WFA was increased, and colocalized distributions were shifted to the right ($D = 0.2689$, $p < 0.0001$) in ASD groups compared with SS controls. Lastly, 6 hr ASD rats had significantly higher and rightward-shifted WFA staining around cells colocalizing with 8-oxo-dG and PV ($D = 0.1928$, $p < 0.005$) compared with SS controls. In contrast to the changes in intensity of 8-oxo-dG, PV, and WFA staining, the number of prelimbic PFC neurons stained with these labels was only significantly elevated for 8-oxo-dG staining between 6 hr ASD-treated rats and SS controls in the prelimbic PFC (Table 2).

Extended sleep fragmentation: SS versus 12 hr ASD

We found that 12 hr ASD reduced the time spent in SWS (32%) relative to SS controls (54%; Table 3; Figure 5A). Time spent in REMS was also reduced by ASD (2%) relative to SS controls (16%), although this near-abolition of REMS was not significant with Bonferroni correction (Table 3; Figure 5B). The loss of sleep was paralleled by a significant increase in time spent in quiet wake during ASD (23%) relative to SS controls (16%; Table 3). Because this experiment was terminated without recovery sleep, the EEG response to sleep loss is not reported.

The intensity of single-labeled cells staining for 8-oxo-dG, PV, and WFA was assessed in both the prelimbic PFC (Figure 6) and OFC (Figure 7) in rats subjected to 12 hr ASD and in SS controls. In the prelimbic PFC, 12 hr ASD increased the intensity of 8-oxo-dG ($D = 0.1261$, $p < 0.0001$), but not PV or WFA (Figure 6A) compared with SS control rats. Twelve hour ASD produced a rightward shift in the intensity of 8-oxo-dG ($D = 0.1261$, $p < 0.0001$), but not in the intensity of PV or WFA compared with rats in the SS condition (Figure 6B).

In the prelimbic PFC, the intensity of 8-oxo-dG was elevated and rightward-shifted in PV cells ($D = 0.1978$, $p < 0.0001$) and in cells surrounded by WFA ($D = 0.1649$, $p < 0.0001$) following ASD treatment (Figure 6, C and D). Additionally, PV intensity colocalizing with 8-oxo-dG ($D = 0.0950$, $p < 0.05$) or WFA ($D = 0.1063$, $p < 0.05$) in the prelimbic PFC was increased, and colocalized distributions where shifted to the right in 12 hr ASD groups compared with SS control conditions. PV+ cells showed a 23% increase in 8-oxo-dG staining following 12 hr ASD, compared with controls, whereas PV– cells only increased 8-oxo-dG staining by 16% following 12 hr ASD. 8-oxo-dG staining intensity in PV+ cells was 50% higher than in PV– cells for 12 hr sleep disrupted rats and 40% higher in controls. No significant differences were found in WFA intensity surrounding 8-oxo-dG or PV cells.

Triple-labeled intensities for 8-oxo-dG, PV, and WFA were also affected by ASD treatment. In the prelimbic PFC, the intensity of 8-oxo-dG colocalizing with both PV and WFA was significantly increased and distributions were shifted upward ($D = 0.2164$, $p < 0.0001$) in ASD-treated rats compared with controls (Figure 6, E and F). Similarly, ASD treatment increased the intensity and upward-shifted PV that colocalized with both 8-oxo-dG and WFA ($D = 0.1161$, $p < 0.001$). No significant changes were found for WFA intensity around cells triple-labeled for 8-oxo-dG, PV, and WFA. Again, in contrast to the changes in the intensity of these markers, the number of prelimbic PFC neurons with each individual label (8-oxo-dG, PV, and WFA) did not differ by treatment (12 hr ASD vs. SS). Additionally, only the number of 8-oxo-dG–stained cells was significant elevated in 12 hr ASD-treated rats, compared with SS controls in the prelimbic PFC (Table 4).

In the OFC, there were fewer differences in the intensities of 8-oxo-dG, PV, and WFA (Figure 7) following 12 hr ASD treatment compared with those changes in the prelimbic PFC. Within the OFC, only the intensity of 8-oxo-dG was elevated in ASD compared with SS rats ($D = 0.03145$, $p < 0.0001$; Figure 7A). The number of OFC neurons with each individual label (8-oxo-dG, PV, and WFA) did not differ by treatment (12 hr ASD vs. SS). Additionally, only the number of 8-oxo-dG stained cells was significantly

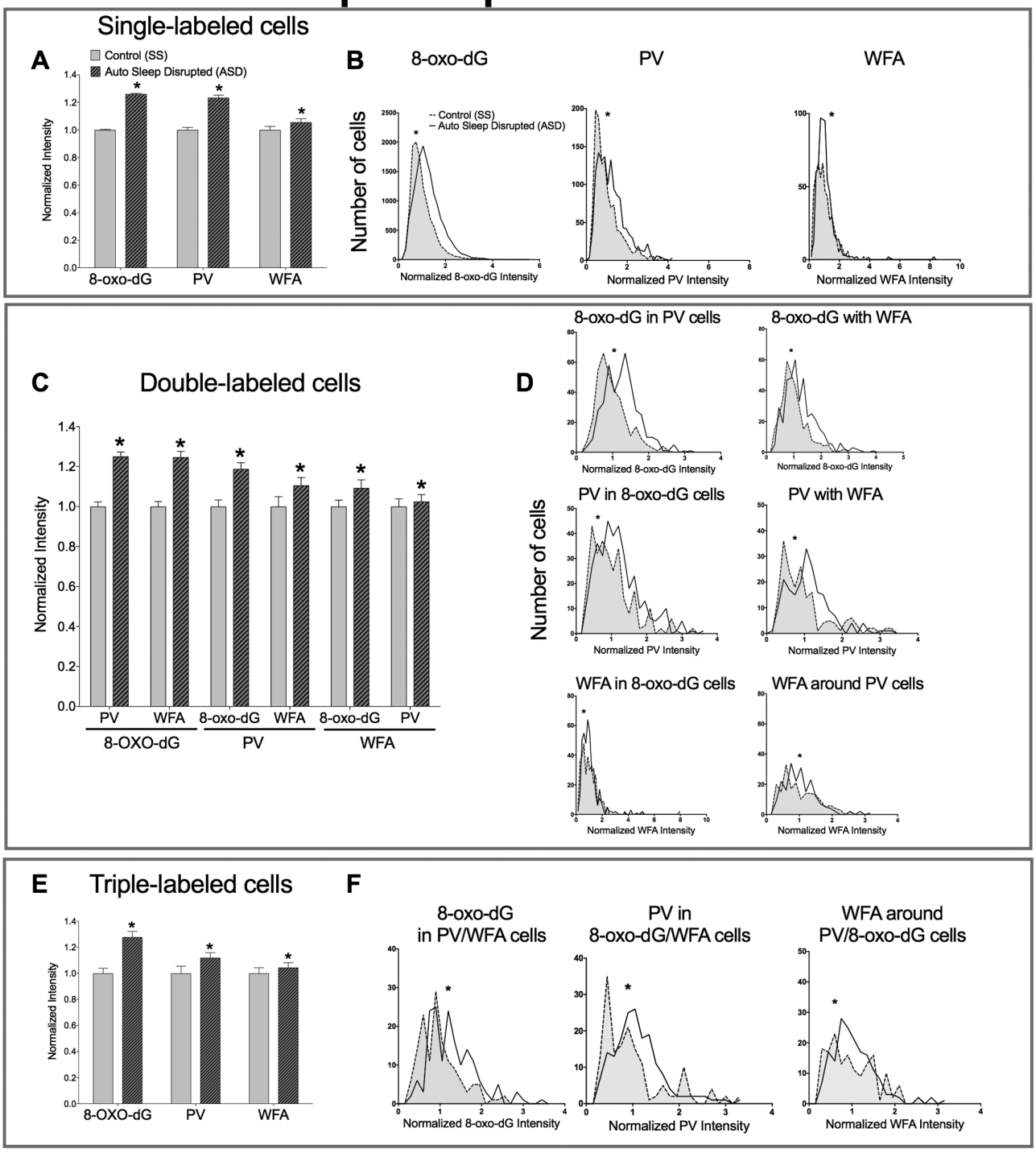

Figure 4. Distributions and mean intensities of histological markers in the prelimbic PFC following SS or 6 hr ASD conditions. (A) Within the prelimbic PFC, 8-oxo-dG, PV, and WFA intensities were significantly greater in ASD rats, compared with SS rats. (B) 6 hr ASD led to a significant change in 8-oxo-dG, PV, and WFA intensity distributions, compared with rats in the SS condition. (C) 8-oxo-dG intensity was significantly elevated following ASD treatment when identified to colocalize with PV or WFA staining in the prelimbic PFC. Prelimbic PFC PV intensity colocalizing with 8-oxo-dG was significantly higher in ASD-treated rats than in SS rats. Additionally, WFA intensities were elevated around 8-oxo-dG and PV neurons in rats experiencing ASD, compared with SS. (D) 6 hr ASD significantly altered 8-oxo-dG intensity distributions on cells colocalizing with PV and WFA, compared with SS. Similarly, ASD altered PV intensity distributions, compared with SS conditions, when colocalizing with 8-oxo-dG or WFA staining. Lastly, WFA labeled populations colocalizing with 8-oxo-dG or PV distributions in ASD rats significantly differed from rats in the SS condition. (E) Within the prelimbic PFC, 8-oxo-dG labeling that colocalized with both PV and WFA was significantly more intense in ASD-treated rats. PV staining that colocalized with both 8-oxo-dG and WFA was significantly more intense in ASD-treated rats. Similarly, 8-oxo-dG and PV neurons that were surrounded by WFA were significantly more intense in ASD-treated rats, compared with SS rats. (F) 6 hr ASD resulted in a significant shift in 8-oxo-dG intensity distributions on cells colocalizing with PV and WFA, compared with SS groups. ASD also shifted the PV intensity distribution, compared with SS conditions, when colocalizing with 8-oxo-dG and WFA labeling. Lastly, the distribution of WFA intensity in populations colocalizing with 8-oxo-dG and PV significantly differed between SS and ASD conditions. $N = 4$, $^{*}p < 0.05$ for the difference between ASD and SS means.

Table 2. Number of stained cells counted in images from PFC region of rats experiencing 6 hr ASD versus 6 hr of SS

Tmt	Stain	Mean Cell N	SEM
SS	8-oxo	363.4012	63.20796
ASD	8-oxo*	431.5333	92.15221
SS	PV	35.7268	8.58648
ASD	PV	37.8385	9.80665
SS	WFA	12.5689	1.16322
ASD	WFA	20.9547	7.14017
SS	Double-labeled_8-oxo_co-occurring_with_PV	12.3353	3.37286
ASD	Double-labeled_8-oxo_co-occurring_with_PV	12.1201	2.97161
SS	Double-labeled_8-oxo_co-occurring_with_WFA	7.6607	1.38806
ASD	Double-labeled_8-oxo_co-occurring_with_WFA	14.7898	5.00631
SS	Double-labeled_PV_co-occurring_with_8-oxo	10.0972	2.34678
ASD	Double-labeled_PV_co-occurring_with_8-oxo	10.2999	2.55425
SS	Double-labeled_PV_co-occurring_with_WFA	6.0456	1.78787
ASD	Double-labeled_PV_co-occurring_with_WFA	6.4017	1.82483
SS	Double-labeled_WFA_co-occurring_with_8-oxo	8.0397	1.49684
ASD	Double-labeled_WFA_co-occurring_with_8-oxo	15.5131	5.1448
SS	Double-labeled_WFA_co-occurring_with_PV	6.1369	1.77212
ASD	Double-labeled_WFA_co-occurring_with_PV	6.4329	1.81061
SS	Triple-labeled_8-oxo	4.3075	0.95501
ASD	Triple-labeled_8-oxo	5.5768	1.57678
SS	Triple-labeled_PV	4.8492	1.31126
ASD	Triple-labeled_PV	7.7842	3.34788
SS	Triple-labeled_WFA	4.8492	1.31126
ASD	Triple-labeled_WFA	5.9092	1.79003

*$p < 0.05$ difference between SD and SS, Fisher's LSD.

Table 3. Percentage of time spent in each sleep state during a 12 hr ASD session vs. 12 hr of SS (ZT0–12)

State	ASD (% of total time)	SS (% of total time)
SWS	32 ± 4*	54 ± 3
REMS	2 ± 1	16 ± 1
Quiet Wake	23 ± 3*	16 ± 2
Intermediate Wake	22 ± 5	6 ± 1
Active Wake	21 ± 3	8 ± 1

*$p < 0.05$ difference between ASD and SS, Student's T with Bonferroni correction.

elevated in 12 hr ASD-treated rats, compared with SS controls in the OFC (Table 5). Figure 8 shows photomicrographs of 8-oxo-dG, PV, and WFA staining in the prelimbic PFC in control and 12 hr SD rats.

Discussion

We show here for the first time that biochemical markers for oxidative stress are elevated in PV cells during enforced wakefulness. The accumulation of oxidative stress in the brain shown here and elsewhere [5–7, 39] is likely a consequence of the high rate of mitochondrial energy generation during wake relative to sleep (reviewed in Refs. 40 and 41). Sleep deprivation alters markers of mitochondrial metabolism, including increased mitochondrial volume [42], protein [43], and electron microscopic [44] markers. Increased mitochondrial energy production via oxidation–reduction reactions may lead to oxidative stress, and here, SD increased markers of oxidative stress in the prelimbic PFC of rats in both the 6 and 12 hr ASD conditions when compared with spontaneously sleeping rats. Additionally, both 6 and 12 hr ASD resulted in increased PV staining intensity (Figures 4 and 6) and right-shifted PV intensity distributions.

Our data demonstrate that oxidative stress was increased following 6 and 12 hr SD in PV-positive neurons, and that PV signal intensity increased in neurons undergoing oxidative stress in SD conditions. The high-frequency activity of PV cells during wakefulness, concomitant with their essential role in generating gamma activity [28], may increase their metabolic demands and vulnerability to oxidative stress relative to other neuronal populations. PNNs are composed of chondroitin sulfate proteoglycans (CSPGs), in combination with tenascin-R, hyaluronan, and link proteins such as Crtl1 [45]. These are components of the extracellular matrix generated by neurons and glia that ensheath neuronal cell bodies and proximal dendrites but that are excluded from the synaptic cleft [45, 46]. We recently found that in the prelimbic PFC, approximately 75% of PV interneurons are surrounded by PNNs [22], in agreement with prior work showing that the vast majority of PNN-positive cells are PV cells, and the vast majority of PV cells are PNN-positive [47, 48]. Additionally, intracerebral administration of chondroitinase-ABC to disrupt PNNs results in increased histological detection of oxidative stress markers in PV cells [15] but not cell death [22]. In postmortem assays of human brains, cerebral cortical neurons that were surrounded by PNNs exhibited reduced lipofuscin accumulation, a marker of oxidative stress, compared with those devoid of PNNs [24]. This protective effect of PNNs is likely due to their enrichment for chondroitin sulfate, which serves as a substrate for oxidative buffering reactions [25] and reverses measures of oxidative stress in neuron-derived SH-SY-5Y neuroblastoma cells in vitro [26]. Nonetheless, we found that in SD rats, oxidative stress markers increased by 25% and 23% in PV neurons after 6 and 12 hr sleep deprivation, respectively, regardless of whether the PV cells were surrounded by PNNs. It is possible that PNNs

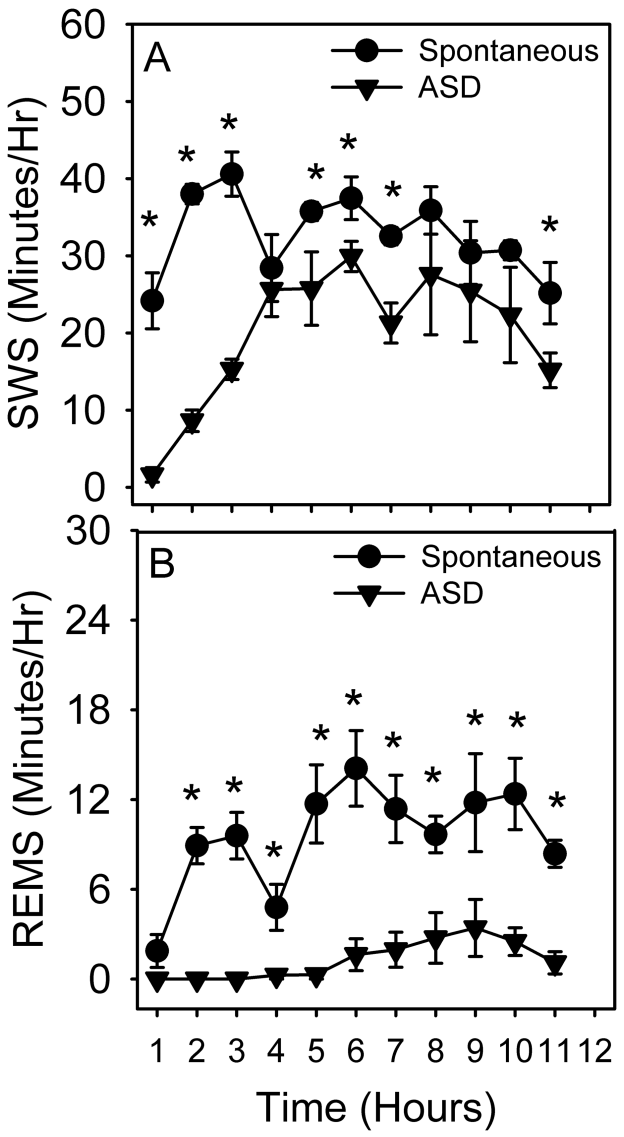

Figure 5. SWS and REMS recorded during 12 hr ASD or SS in undisturbed conditions. Data from the last hour are not shown because this is when the animals were euthanized. (A) Time spent in SWS during the 12 hr SD session. (B) Time spent in REMS during the 12 hr SD session. *$p < 0.05$, Fisher's LSD, ASD vs. baseline.

do buffer against oxidative stress during shorter bouts of wakefulness, but the current observations do not point to a protective antioxidant role for PNNs during protracted wakefulness. In PV-negative cells, the increase in oxidative stress was still significantly higher following sleep disruption, compared with SS rats, although the increase was greater after 6 hr of SD, compared with 12 hr of sleep deprivation. Additionally, we found that in 12 hr sleep-disrupted rats, 8-oxo-dG staining in PV-positive cells was significantly higher (by 50%) than PV-negative cells, suggesting that PV-containing cells experience higher levels of oxidative stress than less metabolically active cells. However, PV-positive cells also experienced more oxidative stress in non-sleep deprived rats, but the increase in intensity was only 40% higher than PV-negative cells. This suggests that while oxidative stress in fast-spiking PV cells is higher than in PV-negative cells, sleep deprivation will increase oxidative stress in these areas of the brain regardless of PV content.

A wealth of studies implicate sleep in reversal of metabolic demand-driven accumulation of oxidative stress during wake [5–7, 39], reviewed in Ref. 40. PNNs undergo degradation in response to superoxide radical exposure in vitro [26]. This phenomenon has not been documented in the intact brain, but if PNN degradation is a physiological mechanism for oxidative buffering, one might expect it to occur as a consequence of oxidative stress in protracted wake. We have measured diurnal rhythms in PNN intensity that parallel the daily sleep–wake cycle in the brains of animals undergoing SS [49] and accordingly hypothesized that ASD would precipitate PNN degradation. In the current study, 6 hr ASD led to a small but significant increase in PNN intensity. It is possible that the intrusion of sleep into the period of enforced wake was sufficient to reverse any oxidative stress-induced loss of PNNs. Indeed, the impact of 12 hr SD on 8-oxo-dG and PV intensity was not greater than that of 6 hr SD, suggesting that even relatively brief bouts of sleep may offset markers of oxidative stress. Measurement of PNN intensity after total sleep deprivation will be needed to address this possibility.

The current work confirms variability in the redox status of PV neurons as a function of sleep. Metabolically demanding and oxidative stress-vulnerable PV-positive neurons play a central role in maintaining circuit activity that underlies waking cortical activation. Experimental manipulations that either generically induce brain oxidative stress [14] or selectively suppress antioxidant activity in PV cells [15] are disruptive to gamma activity or alter gamma activity in response to stimuli. Therefore, impairments that occur during protracted wake and other states of cerebral oxidative stress are likely secondary effects of extreme metabolic demand on PV cells, the resulting cell type-specific oxidative stress, and subsequent loss of orchestrated gamma activity.

Increased PV expression as a consequence of sleep deprivation is an additional novel observation. PV itself serves to buffer and facilitate the intracellular sequestration of calcium [50]. Elevated PV expression over time awake may be protective against excessive calcium concentrations during protracted periods of PV cell firing. The intensity of PV staining is tightly correlated with the levels of GAD65/67, the rate-limiting enzyme for GABA synthesis [51]. Therefore, SD-induced increases in PV intensity strongly suggest that GAD levels, and thus inhibitory signaling by these GABAergic interneurons, are increased. An increase in this GABAergic inhibition onto pyramidal neurons may underlie some of the cognitive deficits found after SD. Interestingly, PV cells and PNNs are reduced in schizophrenia, and cognitive deficits in schizophrenia have recently been shown to be reduced by oral administration of the antioxidant, N-acetyl cysteine [52].

SD is easily achieved in experimental rodents by applying sensory stimulation. Here, we applied a novel method of SD for the laboratory rat in which an agitator is placed in the base of the rodent's standard home cage. Various automated approaches such as a rotating disk over a pool of water [53] or a treadmill [54] have been applied to minimize the need for experimenter intervention. However, these methods require the rodent to be removed from its home cage and placed into an unfamiliar environment, possibly containing scents from other rodents, which can represent threats or potential mates to the experimental subject. Exposure to environmental novelty can significantly increase plasma corticosterone levels in rats and mice [55, 56]. We believe that elevated stress levels and

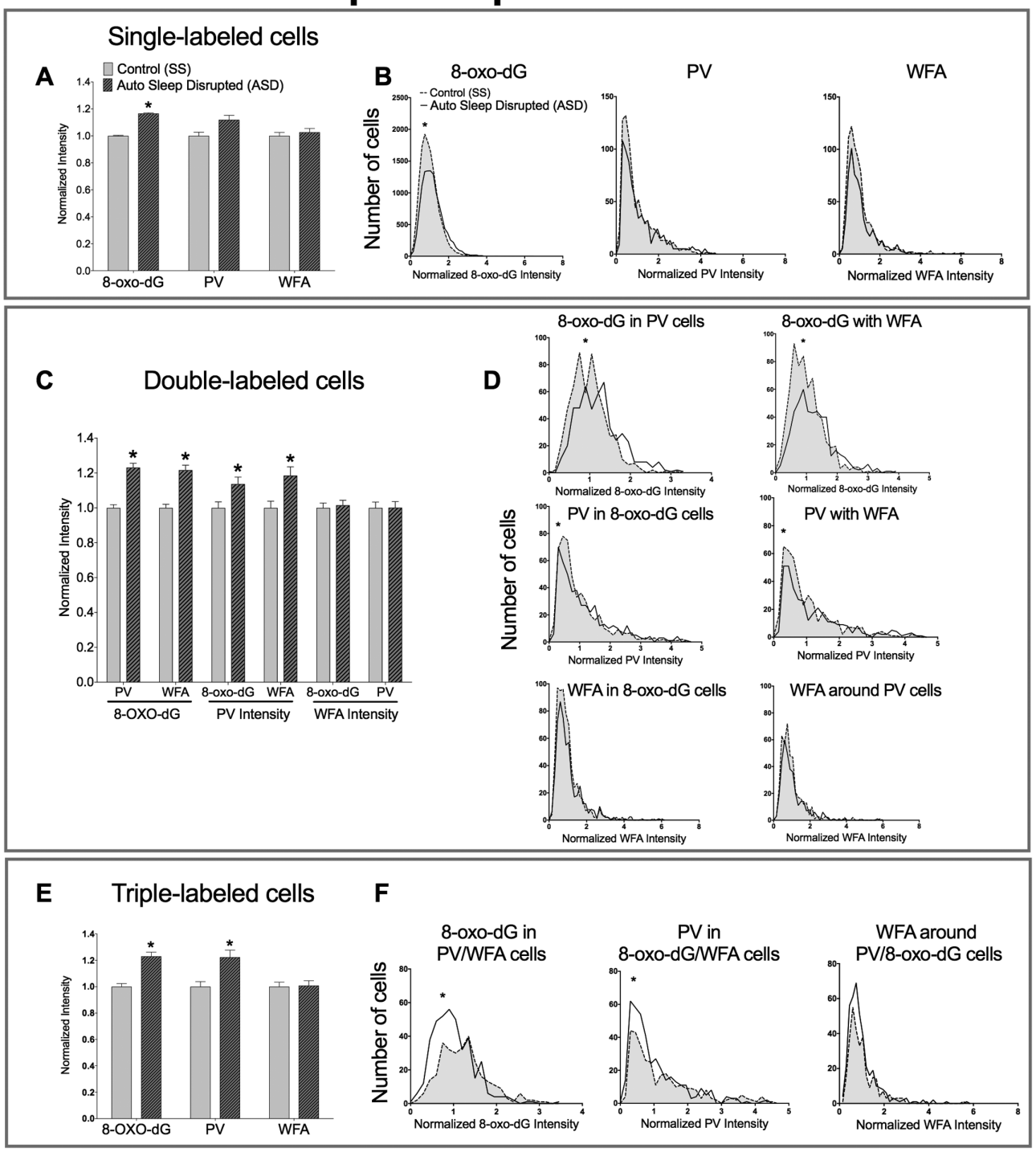

Figure 6. Stain intensities in the prelimbic PFC following SS or 12 hr ASD conditions. (A) Within the prelimbic, 8-oxo-dG and PV intensities were significantly greater in ASD group rats, compared with SS rats. (B) 12 hr ASD led to a significant change in 8-oxo-dG intensity, compared with rats in the SS condition. However, ASD did not significantly alter PV or WFA distributions. (C) 8-oxo-dG intensity was significantly elevated following ASD treatment when identified to colocalize with PV or WFA staining in the prelimbic. Additionally, prelimbic PFC PV intensity that colocalized with 8-oxo-dG or WFA staining was significantly higher in ASD than SS rats. (D) 12 hr ASD significantly altered 8-oxo-dG intensity distributions on cells colocalizing with PV and WFA, compared with controls (SS). Similarly, ASD altered PV intensity distributions, compared with SS conditions, when colocalizing with 8-oxo-dG or WFA staining. However, no significant differences were found in WFA labeled populations colocalizing with 8-oxo-dG or PV distributions. (E) Within the prelimbic PFC, 8-oxo-dG labeling that colocalized with both PV and WFA was significantly more intense in ASD-treated rats. Similarly, PV-labeled cells that colocalized with both 8-oxo-dG and WFA were significantly more intense in ASD than SS rats. (F) 12 hr ASD resulted in a significant shift in 8-oxo-dG intensity distributions on cells colocalizing with PV and WFA, compared with SS groups. ASD also shifted the PV intensity distribution, compared with SS conditions, when colocalizing with 8-oxo-dG and WFA staining. However, no significant differences were found in WFA-labeled populations colocalizing with 8-oxo-dG and PV. $N = 8$, $^*p < 0.05$ for the difference between ASD and SS intensity distributions.

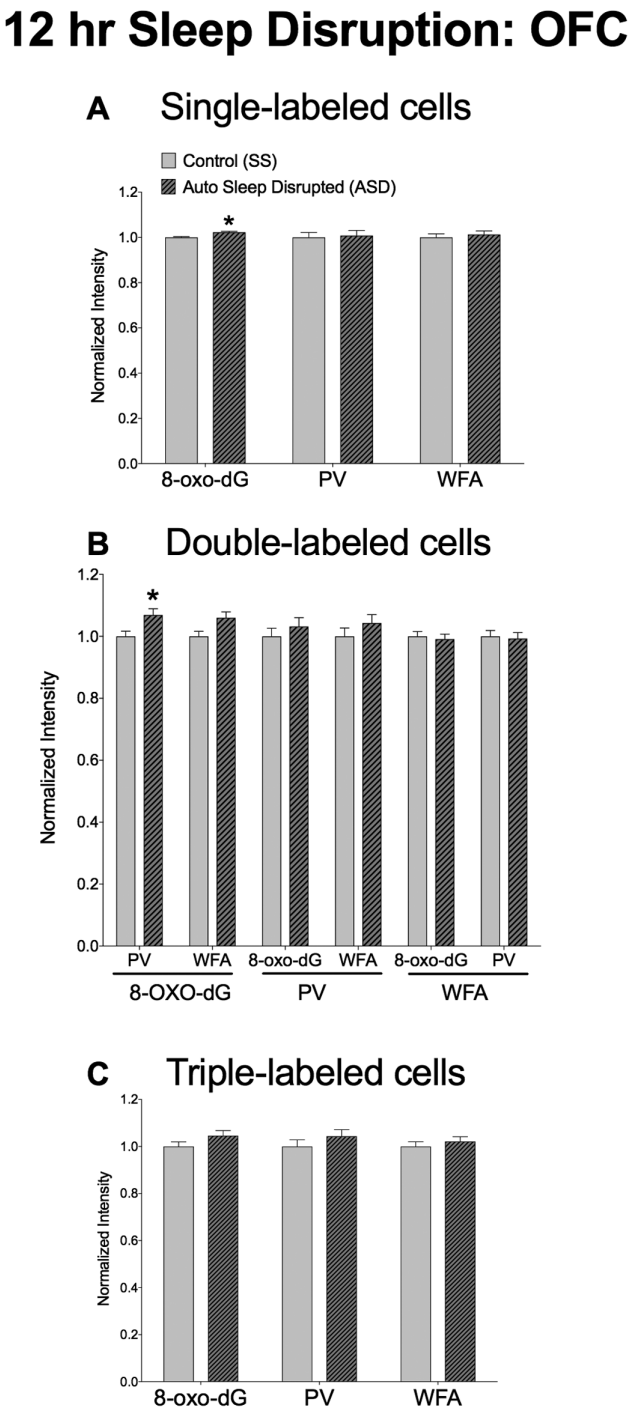

Figure 7. Mean intensities in the OFC following SS or 12 hr ASD conditions. (A) Within the OFC, only 8-oxo-dG intensities significantly differed in ASD group rats, compared with SS rats. (B) 8-oxo-dG intensity was significantly elevated following ASD treatment when identified to colocalize with PV staining in the OFC. (C) However, no differences were found between ASD and SS treatment groups in OFC intensities that colocalized with both other labels. $N = 8$, $^*p < 0.05$ for the difference between ASD and SS mean.

novelty-associated learning can confound or mask effects of sleep deprivation at the cellular or molecular levels. Therefore, elimination of novel environmental confounds through our ASD method may improve the reliability and reproducibility of SD data. Additionally, use of the rodent's home cage eliminates the need for additional chamber cleaning between experiments because the home cage and agitator can be washed normally by vivarium husbandry technicians. The automated SD apparatus used here can be applied to future studies, with the advantage that ASD is delivered in the animal's home cage.

The efficacy of the ASD method was validated by measuring the polysomnographic response to 6 or 12 hr SD with this method in comparison to the GHSD method. Both the ASD and GHSD methods decreased REMS compared with controls, and REMS was not found to differ between ASD and GHSD conditions. Additionally, both ASD and GHSD reduced time spent in SWS. However, rats in the ASD condition spent more time in SWS during hours 2–6 than rats in the GHSD condition. These findings indicate that ASD using the Sleep Fragmentation Platform performed as well as GHSD to reduce REMS, but not SWS. Both SD conditions produced rebound sleep following the 6 hr SD session. SWA during SWS was elevated relative to baseline during the entirety of the 6 hr recovery sleep opportunity after 6 hr SD, but it was elevated to a greater extent in GHSD than in ASD during hours 1–2 post-SD. After this time, SWA was elevated to the same extent in both GHSD and ASD relative to baseline. By this measure, ASD may be said to be less effective than GHSD in increasing sleep drive, as is true for other ASD methods [25].

Limitations

We found a greater number of differences in intensity and distribution of PV intensities when measuring the responses to 6 hr SD compared with those to the 12 hr SD. One possibility is that differences are derived from the absence of tethering (for EEG) in the rats in the 6 hr SD IHC study. However, rats in the sleep study were adapted to the tethers for 24 hr, which is standard in the sleep field, so it does not seem likely to explain the differences. Second, in the 6 hr SD IHC group, it is possible that rats slept differently compared with those tethered to the EEG system. However, we monitored each rat's behavior throughout the entire 6 hr SD period using a camera placed above the cage. We did not observe any overt signs of sleep, although we could not rule out that rats may have entered into short periods of SWS, as was observed in EEG recordings. Overall, the findings from the 6 hr SD group were highly similar to those from the 12 hr SD group, underlining the impact of prolonged wakefulness on neurons within areas of the cortex that drive cognition and decision-making behavior. Finally, we did not separately test whether there were time-of-day effects on the intensity or number of cells expressing 8-oxo-dG, PV, or WFA. It is possible that the expression of these proteins and PNNs is influenced by circadian or diurnal rhythms, which SD may have disrupted. Superimposing SD effects onto any circadian rhythm effects during ZT0–ZT6 vs. ZT0–ZT12 may have either masked or amplified some of the differences between SD groups and SS controls. Future studies would require SD to be conducted across all phases of the circadian cycle to fully address this issue.

Conclusion

Our novel method for ASD effectively reduced both SWS and REMS measures of sleep in rats compared with controls. GHSD reduced SWS to a greater extent than did the automated platform, similar to reports using other ASD methods available [32]. However, a main advantage of the ASD method used here is that it

Table 4. Number of stained cells counted in images from PFC region of rats experiencing 12 hr ASD versus 6 hr of SS

Tmt	Stain	Mean Cell N	SEM
SS	8-oxo	532.7396	11.89876
ASD	8-oxo*	553.3334	13.10269
SS	PV	30.7083	2.63952
ASD	PV	33.4584	4.39979
SS	WFA	27.1417	2.27989
ASD	WFA	27.8334	3.15714
SS	Double-labeled_8-oxo_co-occurring_with_PV	21.7709	1.70559
ASD	Double-labeled_8-oxo_co-occurring_with_PV	24.625	0.49709
SS	Double-labeled_8-oxo_co-occurring_with_WFA	25	1.89418
ASD	Double-labeled_8-oxo_co-occurring_with_WFA	23.7917	1.44077
SS	Double-labeled_PV_co-occurring_with_8-oxo	19.9063	2.6259
ASD	Double-labeled_PV_co-occurring_with_8-oxo	23.5417	2.88464
SS	Double-labeled_PV_co-occurring_with_WFA	16.6771	2.63789
ASD	Double-labeled_PV_co-occurring_with_WFA	17.75	2.91031
SS	Double-labeled_WFA_co-occurring_with_8-oxo	25.3333	1.58552
ASD	Double-labeled_WFA_co-occurring_with_8-oxo	27.125	2.82299
SS	Double-labeled_WFA_co-occurring_with_PV	16.6771	2.61409
ASD	Double-labeled_WFA_co-occurring_with_PV	17.7917	2.89745
SS	Triple-labeled_8-oxo	15.5104	2.28627
ASD	Triple-labeled_8-oxo	15	2.15057
SS	Triple-labeled_PV	15.9896	2.22493
ASD	Triple-labeled_PV	16.6667	3.21814
SS	Triple-labeled_WFA	15.9896	2.22493
ASD	Triple-labeled_WFA	19.3333	2.49166

*$p < 0.05$ difference between SD and SS, Fisher's LSD.

Table 5. Number of stained cells counted in images from OFC region of rats experiencing 12 hr ASD versus 6 hr of SS

Tmt	Stain	Mean Cell N	SEM
SS	8-oxo	693.6191	27.02332
ASD	8-oxo*	748.9167	58.75593
SS	PV	43.5417	7.07936
ASD	PV	45.875	7.36434
SS	WFA	43.8155	2.66426
ASD	WFA	47.9584	4.87926
SS	Double-labeled_8-oxo_co-occurring_with_PV	30.5893	4.45198
ASD	Double-labeled_8-oxo_co-occurring_with_PV	32	4.83668
SS	Double-labeled_8-oxo_co-occurring_with_WFA	41.5298	2.27672
ASD	Double-labeled_8-oxo_co-occurring_with_WFA	47.7917	5.80044
SS	Double-labeled_PV_co-occurring_with_8-oxo	30.2619	5.37063
ASD	Double-labeled_PV_co-occurring_with_8-oxo	29.6905	4.8613
SS	Double-labeled_PV_co-occurring_with_WFA	26.8274	5.39038
ASD	Double-labeled_PV_co-occurring_with_WFA	28.8988	5.09262
SS	Double-labeled_WFA_co-occurring_with_8-oxo	43.8334	3.66224
ASD	Double-labeled_WFA_co-occurring_with_8-oxo	45.2798	5.04505
SS	Double-labeled_WFA_co-occurring_with_PV	26.8274	5.39038
ASD	Double-labeled_WFA_co-occurring_with_PV	29.0238	5.04017
SS	Triple-labeled_8-oxo	23.8988	4.32168
ASD	Triple-labeled_8-oxo	28.7083	4.07986
SS	Triple-labeled_PV	24.5655	4.38768
ASD	Triple-labeled_PV	28.5417	4.89206
SS	Triple-labeled_WFA	24.5655	4.38768
ASD	Triple-labeled_WFA	29.25	4.40195

*$p < 0.05$ difference between SD and SS, Fisher's LSD.

can be used in the animal's standard home cage and alleviate any novelty-induced changes in sleep. Thus, the Sleep Fragmentation Platform used here can be applied for automated SD in future studies. We found that WFA was slightly elevated in neurons following 6 hr, but not 12 hr SD, likely indicating a transient increase in PNN content. Additionally, we found an increase in oxidative stress in neurons following 6 and 12 hr SD. This increase was particularly apparent in PV+, PV–, and WFA neurons after 6 hr SD. This is consistent with previous studies that demonstrate increases in oxidative stress with prolonged wakefulness [39]. Additional work on the biological basis for the negative health impacts of SD may offer mitigation strategies, such as antioxidant treatment.

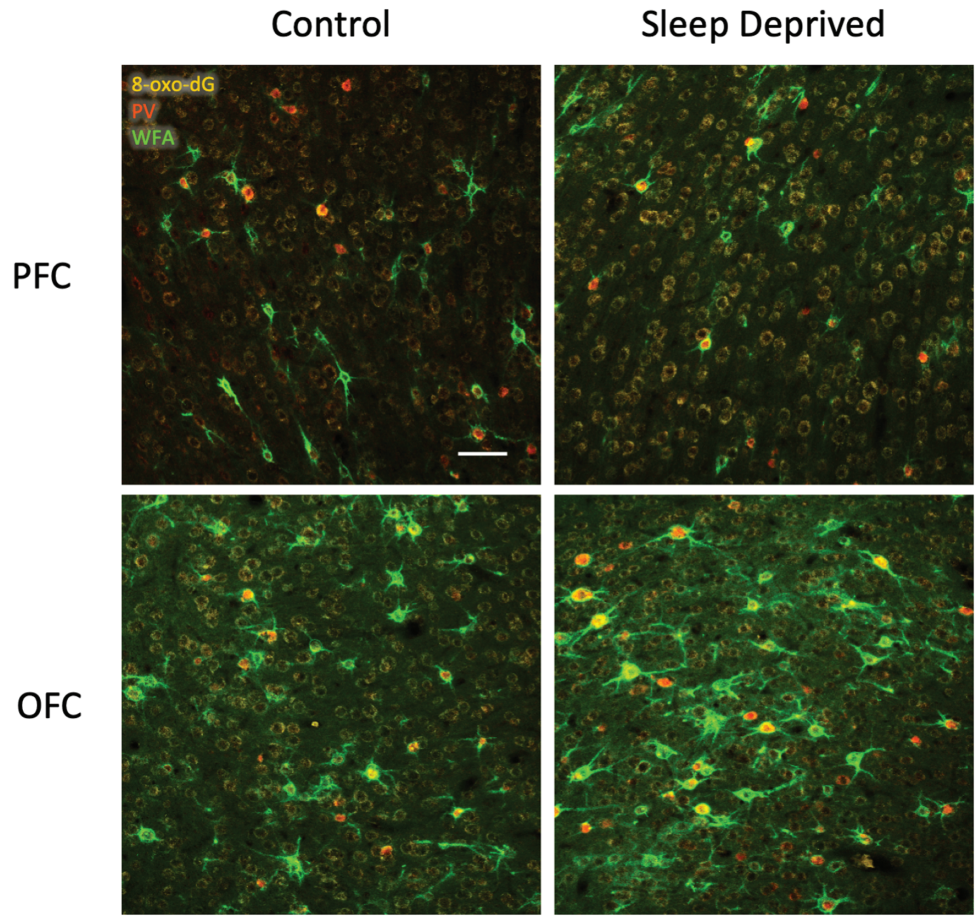

Figure 8. Representative confocal images of histological markers in the prelimbic PFC and OFC following SS or 12 hr ASD conditions. WFA shown in green stain, PV shown in cells filled with red stain (few cells), and 8-oxo-dG shown in yellow outlining cells (many cells). Scale bar = 50 µm.

Funding

This work was supported by National Institutes of Health DA033404 and DA040965 (to B.A.S.) and Washington State University Commercialization Gap Fund (FY2017), Washington State University Postdoctoral Alcohol and Drug Abuse Research Program (FY2016), and NSF ICORPS Award# 1547873 (to J.H.H.—trainee).

Conflict of interest statement. J.H.H., R.P.T., and B.A.S. are listed as inventors on Washington State University patent application wsu-oc-1717 "trolley for the automation of sleep disruption." J.H.H. and B.A.S. are listed as inventors on the Washington State University analysis program, Pipsqueak. J.H.H. is a majority stake holder in Rewire Neuroscience, LLC, the licensing partner of this Sleep Fragmentation Platform, and Pipsqueak technologies. J.P.W., P.N.B., and W.C.C. performed all polysomnographic experimentation, data collection, and data analysis and have no financial interest in any of the above-listed entities. The authors do not perceive these relationships to have had an influence on this report.

References

1. Ford ES. Habitual sleep duration and predicted 10-year cardiovascular risk using the pooled cohort risk equations among US adults. *J Am Heart Assoc.* 2014;**3**(6):e001454.
2. Liu Z, *et al.* Prefrontal cortex to accumbens projections in sleep regulation of reward. *J Neurosci.* 2016;**36**(30):7897–7910.
3. Romcy-Pereira R, *et al.* Distinct modulatory effects of sleep on the maintenance of hippocampal and medial prefrontal cortex LTP. *Eur J Neurosci.* 2004;**20**(12):3453–3462.
4. Trivedi MS, *et al.* Short-term sleep deprivation leads to decreased systemic redox metabolites and altered epigenetic status. *PLoS One.* 2017;**12**(7):e0181978.
5. Ramanathan L, *et al.* Short-term total sleep deprivation in the rat increases antioxidant responses in multiple brain regions without impairing spontaneous alternation behavior. *Behav Brain Res.* 2010;**207**(2):305–309.
6. Ramanathan L, *et al.* Sleep deprivation under sustained hypoxia protects against oxidative stress. *Free Radic Biol Med.* 2011;**51**(10):1842–1848.
7. Panossian L, *et al.* SIRT1 regulation of wakefulness and senescence-like phenotype in wake neurons. *J Neurosci.* 2011;**31**(11):4025–4036.
8. Ivanov A, *et al.* Critical state of energy metabolism in brain slices: the principal role of oxygen delivery and energy substrates in shaping neuronal activity. *Front Neuroenergetics.* 2011;**3**:9.
9. Schönfeld P, *et al.* Why does brain metabolism not favor burning of fatty acids to provide energy? Reflections on disadvantages of the use of free fatty acids as fuel for brain. *J Cereb Blood Flow Metab.* 2013;**33**(10):1493–1499.

10. Gaykema RP, *et al*. Characterization of excitatory and inhibitory neuron activation in the mouse medial prefrontal cortex following palatable food ingestion and food driven exploratory behavior. *Front Neuroanat*. 2014;**8**:60.
11. Staiger JF, *et al*. Excitatory and inhibitory neurons express c-Fos in barrel-related columns after exploration of a novel environment. *Neuroscience*. 2002;**109**(4):687–699.
12. Buzsáki G, *et al*. Mechanisms of gamma oscillations. *Annu Rev Neurosci*. 2012;**35**:203–225.
13. Grønli J, *et al*. Beta EEG reflects sensory processing in active wakefulness and homeostatic sleep drive in quiet wakefulness. *J Sleep Res*. 2016;**25**(3):257–268.
14. Galow LV, *et al*. Energy substrates that fuel fast neuronal network oscillations. *Front Neurosci*. 2014;**8**:398.
15. Cabungcal JH, *et al*. Perineuronal nets protect fast-spiking interneurons against oxidative stress. *Proc Natl Acad Sci USA*. 2013;**110**(22):9130–9135.
16. Pizzorusso T, *et al*. Reactivation of ocular dominance plasticity in the adult visual cortex. *Science*. 2002;**298**(5596):1248–1251.
17. Galtrey CM, *et al*. The role of chondroitin sulfate proteoglycans in regeneration and plasticity in the central nervous system. *Brain Res Rev*. 2007;**54**(1):1–18.
18. Fawcett J. Molecular control of brain plasticity and repair. *Prog Brain Res*. 2009;**175**:501–509.
19. Gogolla N, *et al*. Perineuronal nets protect fear memories from erasure. *Science*. 2009;**325**(5945):1258–1261.
20. Mauney SA, *et al*. Developmental pattern of perineuronal nets in the human prefrontal cortex and their deficit in schizophrenia. *Biol Psychiatry*. 2013;**74**(6):427–435.
21. Xue YX, *et al*. Depletion of perineuronal nets in the amygdala to enhance the erasure of drug memories. *J Neurosci*. 2014;**34**(19):6647–6658.
22. Slaker M, *et al*. Removal of perineuronal nets in the medial prefrontal cortex impairs the acquisition and reconsolidation of a cocaine-induced conditioned place preference memory. *J Neurosci*. 2015;**35**(10):4190–4202.
23. Yutsudo N, *et al*. Involvement of chondroitin 6-sulfation in temporal lobe epilepsy. *Exp Neurol*. 2015;**274**(Pt B):126–133.
24. Morawski M, *et al*. Perineuronal nets potentially protect against oxidative stress. *Exp Neurol*. 2004;**188**(2):309–315.
25. Campo GM, *et al*. Reduction of DNA fragmentation and hydroxyl radical production by hyaluronic acid and chondroitin-4-sulphate in iron plus ascorbate-induced oxidative stress in fibroblast cultures. *Free Radic Res*. 2004;**38**(6):601–611.
26. Rees MD, *et al*. Hypochlorite and superoxide radicals can act synergistically to induce fragmentation of hyaluronan and chondroitin sulphates. *Biochem J*. 2004;**381**(Pt 1):175–184.
27. Womelsdorf T, *et al*. The role of neuronal synchronization in selective attention. *Curr Opin Neurobiol*. 2007;**17**(2):154–160.
28. Sohal VS, *et al*. Parvalbumin neurons and gamma rhythms enhance cortical circuit performance. *Nature*. 2009;**459**(7247):698–702.
29. Institute of Laboratory Animal Resources NRC. *Guide for Care and Use of Laboratory Animals*. Washington, DC: National Academy Press; 1996.
30. Wisor JP, *et al*. Armodafinil, the R-enantiomer of modafinil: wake-promoting effects and pharmacokinetic profile in the rat. *Pharmacol Biochem Behav*. 2006;**85**(3):492–499.
31. Morairty SR, *et al*. The wake-promoting effects of hypocretin-1 are attenuated in old rats. *Neurobiol Aging*. 2011;**32**(8):1514–1527.
32. Wisor JP, *et al*. Toll-like receptor 4 is a regulator of monocyte and electroencephalographic responses to sleep loss. *Sleep*. 2011;**34**(10):1335–1345.
33. Wisor JP, *et al*. Quantification of short-term slow wave sleep homeostasis and its disruption by minocycline in the laboratory mouse. *Neurosci Lett*. 2011;**490**(3):165–169.
34. Rempe MJ, *et al*. An automated sleep state classification algorithm for quantification of sleep-state timing and sleep-dependent dynamics of electroencephalographic and cerebral metabolic parameters. *Nat Sci Sleep*. 2015;**7**:85–99.
35. Slaker M, *et al*. Impact of environmental enrichment on perineuronal nets in the prefrontal cortex following early and late abstinence from sucrose self-administration in rats. *PLoS One*. 2016;**11**(12):e0168256.
36. Grønli J, *et al*. A rodent model of night shift work induces short- and long-term sleep and electroencephalographic disturbances. *J Biol Rhythms*. 2017;**32**(1):48–63.
37. Grønli J, *et al*. Sleep homeostatic and waking behavioral phenotypes in Egr3-deficient mice associated with serotonin receptor 5-HT2 deficits. *Sleep*. 2016;**39**(12):2189–2199.
38. Slaker ML, *et al*. A standardized and automated method of perineuronal net analysis using Wisteria floribunda agglutinin staining intensity. *IBRO Rep*. 2016;**1**:54–60.
39. Silva RH, *et al*. Role of hippocampal oxidative stress in memory deficits induced by sleep deprivation in mice. *Neuropharmacology*. 2004;**46**(6):895–903.
40. Wisor JP. A metabolic-transcriptional network links sleep and cellular energetics in the brain. *Pflugers Arch*. 2012;**463**(1):15–22.
41. Aalling NN, *et al*. Cerebral metabolic changes during sleep. *Curr Neurol Neurosci Rep*. 2018;**18**(9):57.
42. de Vivo L, *et al*. Loss of sleep affects the ultrastructure of pyramidal neurons in the adolescent mouse frontal cortex. *Sleep*. 2016;**39**(4):861–874.
43. Ren J, *et al*. Quantitative proteomics of sleep-deprived mouse brains reveals global changes in mitochondrial proteins. *PLoS One*. 2016;**11**(9):e0163500.
44. Zhao H, *et al*. Frontal cortical mitochondrial dysfunction and mitochondria-related β-amyloid accumulation by chronic sleep restriction in mice. *Neuroreport*. 2016;**27**(12):916–922.
45. Celio MR, *et al*. Perineuronal nets–a specialized form of extracellular matrix in the adult nervous system. *Brain Res Brain Res Rev*. 1994;**19**(1):128–145.
46. Hockfield S, *et al*. A surface antigen expressed by a subset of neurons in the vertebrate central nervous system. *Proc Natl Acad Sci USA*. 1983;**80**(18):5758–5761.
47. Lensjo KK, *et al*. Differential expression and cell-type specificity of perineuronal nets in hippocampus, medial entorhinal cortex, and visual cortex examined in the rat and mouse. *eNeuro*. 2017;**4**(3):1–18.
48. Härtig W, *et al*. Wisteria floribunda agglutinin-labelled nets surround parvalbumin-containing neurons. *Neuroreport*. 1992;**3**(10):869–872.
49. Harkness JH, *et al*. Net gains and losses: how daily fluctuations in perineuronal net intensity may impact behavior. In: Winter Conference on Brain Research; 2018; Whistler, B.C.
50. Wang W, *et al*. Parvalbumin: targeting calcium handling in cardiac diastolic dysfunction. *Gen Physiol Biophys*. 2009;**28 Spec No Focus**:F3–F6.
51. Donato F, *et al*. Parvalbumin-expressing basket-cell network plasticity induced by experience regulates adult learning. *Nature*. 2013;**504**(7479):272–276.

52. Rapado-Castro M, *et al*. Cognitive effects of adjunctive N-acetyl cysteine in psychosis. *Psychol Med*. 2017;**47**(5):866–876.
53. Everson CA, *et al*. Sleep deprivation in the rat. III. Total sleep deprivation. *Sleep*. 1989;**12**(1):13–21.
54. Tartar JL, *et al*. Hippocampal synaptic plasticity and spatial learning are impaired in a rat model of sleep fragmentation. *Eur J Neurosci*. 2006;**23**(10):2739–2748.
55. Muir JL, *et al*. Corticosterone and prolactin responses to predictable and unpredictable novelty stress in rats. *Physiol Behav*. 1986;**37**(2):285–288.
56. Hennessy MB, *et al*. Nonedible material elicits chewing and reduces the plasma corticosterone response during novelty exposure in mice. *Behav Neurosci*. 1987;**101**(2): 237–245.